# Divertor heat flux mitigation with impurity-seeded standard and snowflake divertors in NSTX.

V. A. Soukhanovskii[1], R. E. Bell[2], A. Diallo[2], S. Gerhardt[2], R. Kaita[2], S. Kaye[2], E. Kolemen[2], B. P. LeBlanc[2], R. Maingi[3], A. McLean[1], J. E. Menard[2], D. Mueller[2], S. F. Paul[2], M. Podesta[2], R. Raman[4], A. L. Roquemore[2], D. D. Ryutov[1], F. Scotti[2]

[1]*Lawrence Livermore National Laboratory, Livermore, CA, USA*
[2]*Princeton Plasma Physics Laboratory, Princeton, NJ, USA*
[3]*Oak Ridge National Laboratory, Oak Ridge, TN, USA*
[4]*University of Washington, Seattle, WA, USA*

**Introduction** At present, the National Spherical Torus Experiment (NSTX) facility is being upgraded to new capabilities to enable physics studies of the spherical tokamak (ST) to advance the ST as a candidate for Fusion Nuclear Science Facility. In the NSTX-U device [1], discharges with $I_p \leq 2$ MA and $P_{NBI} \leq 12.3$ MW and up to 5 s duration are projected to produce steady-state peak divertor heat fluxes in the range 20-30 MW/m$^2$, thereby challenging thermal limits of divertor graphite PFCs [2]. The leading heat flux mitigation candidates for NSTX-U are considered to be the snowflake (SF) divertor geometry [3] and the impurity-seeded radiative divertor (RD) technique, applied to the lower and upper divertors. Experiments in NSTX, a large spherical tokamak with lithium-coated graphite PFCs and high divertor heat flux ($q_{peak} \leq 15$ MW/m$^2$, $q_{\|} \leq 200$ MW/m$^2$ [2]), have produced a basis for NSTX-U projections and initial experiments. In NSTX, operations with both the RD and the SF divertor have been quite successful: a significant reduction of divertor heat flux, from peak values of 4-10 MW/m$^2$ to 0.5-2 MW/m$^2$, simultaneously with good core H-mode confinement characterized by H98(y,2) up to 1, have been demonstrated in 1.0-1.3 s discharges [4, 5, 6, 7, 8, 9]. Owing to a compact divertor with intrinsic carbon radiation, the RD with a partially detached strike point was achieved in NSTX using either (1) divertor $D_2$ injection in the standard (albeit high poloidal magnetic flux expansion $f_m \simeq 20$) divertor geometry, or (2) in the SF divertor geometry, due to its geometric effects. The SF divertor geometry created in NSTX (w.r.t. the standard divertor) offered an up to 100 % higher plasma wetted area (due to a much higher flux expansion), a longer connection length and a larger divertor volume available for volumetric losses [8, 9]. Recent divertor experiments in NSTX enabled a comparison of core and divertor conditions obtained in discharges with the $CD_4$-seeded radiative divertor in the standard divertor geometry, and in the SF divertor geometry. The analysis is focused on compatibility with high-confinement core, and the divertor heat flux and impurity radiation distribution. The quantitative divertor measurements have become possible owing to the new calibrated two-color IR camera [10], multichannel spectroscopy [11] and fast filtered cameras [12].

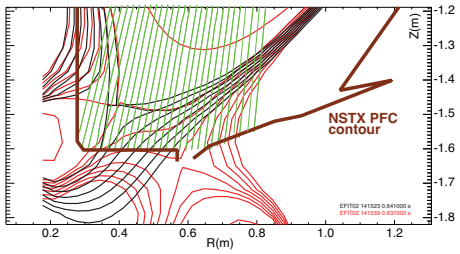


**Figure 1:** *Flux contours of the NSTX lower divertor magnetic configurations: the standard divertor (black lines) and the SF divertor (red lines). Diagnostic views of the cameras and spectrometers are also shown (vertical green lines).*

**Experiment and results** The NSTX experiments were conducted in highly-shaped ($\kappa \simeq 2.1, \delta_{bot} \simeq 0.8$) asymmetric double-null ($drsep \simeq 6-7$mm) configuration, 0.8 MA 4 MW NBI-heated H-mode discharges with $B \times gradB$ direction toward the lower X-point. The SF divertor was formed using three divertor coils starting at about 400-450 ms from a standard divertor discharge [9]. Deuterated methane $CD_4$ was introduced from a lower divertor gas injector. Four typical NBI-heated H-mode dis-

charges will be compared (referring to Figs. 1-4): a reference standard divertor discharge (black traces), a discharge with the SF divertor (red traces), a discharge (standard divertor geometry) with $CD_4$ seeding (green traces), and a discharge with the SF divertor and $CD_4$ seeding (blue traces). The standard and SF divertor geometries that were used are shown in Fig. 1. The scrape-off layer (SOL) power of $P_{SOL} \simeq 3$ MW was obtained for all four discharges using the core power balance estimate as described in Ref. [13].

As a result of $CD_4$ seeding or SF geometry, core confinement metrics were either retained or slightly degraded. Shown in Fig. 2 are time traces of core and divertor measurements in the four NBI-heated H-mode discharges. The SF geometry and $CD_4$ puffing did not affect H-mode access (at 4MW NBI), whereas the confinement characteristics ($W_{MHD} \simeq 250$ kJ, H98(y,2)$\sim 1$, $\tau_E \simeq 65$ ms) were unaffected or reduced by $5-10$ %. Core $T_e$ was reduced from 0.9-1.0 keV to 0.8-0.9 keV. The reference discharge that was run earlier in the day had a lower $n_e$ albeit slightly higher fueling.

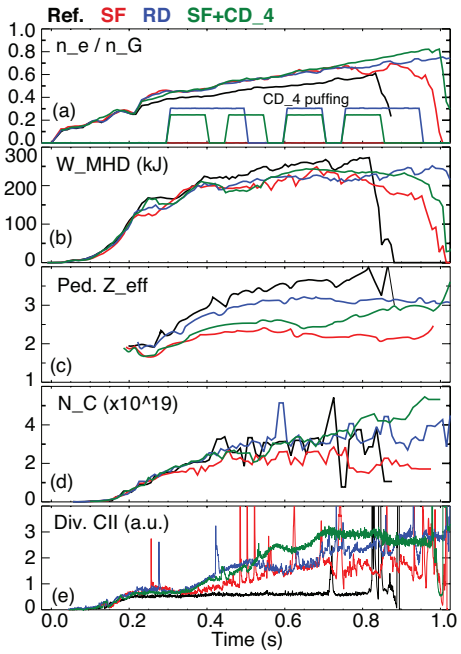


**Figure 2:** Time traces of the four discharges described in text: (a) Greenwald fraction $n_e/n_G$ and divertor gas injection; (b) Plasma stored energy $W_{MHD}$; (c) Pedestal-weighted $Z_{eff}$; (d) core carbon inventory $N_C$; (e) Divertor C II ($\lambda$658.5 nm) intensity.

The core plasma carbon content metrics (e.g., the plasma effective charge $Z_{eff}$ and the total carbon inventory $N_c$ as shown in Fig. 2) were important criteria in the experiment. In general, divertor screening in both the high flux expansion standard divertor and the SF divertor was strong: $CD_4$ puffing from a divertor location did not lead to excessive $Z_{eff}$ and $N_c$ in comparison with the reference discharge. The SF divertor phase had a profound effect on plasma impurity content: both the $Z_{eff}$ and $N_c$ were reduced. The observed reduction was attributed to the reduction of carbon physical sputtering fluxes in the SF divertor (due to very low divertor $T_e$), and to the particle expulsion effect from ELMs that appeared in the SF phase [9]. In the standard divertor H-mode discharge, lithium coatings on lower divertor PFCs reduced recycling and led to modified edge plasma pressure and current profiles and low-$n$ peeling-ballooning mode stabilization [14, 15], as the pedestal stability operating point was close to the peeling boundary. The transition to the SF configuration led to a clear and reproducible destabilization of the ELMs. These large ELMs were classified as Type I, with somewhat irregular frequency of $f = 12-35$ Hz and $\Delta W_{MHD}/W_{MHD}$ in the range 5-10 %. The study of the ELM destabilization in the SF discharges and MHD stability calculations are planned. Interestingly, $CD_4$ puffing into the SF divertor phase apparently led to ELM stabilization again. The discharge scenario with the SF divertor, gas puffing and lithium conditioning, i.e. a high-performance ELM-free discharge without impurity accumulation and reduced divertor heat flux would be an attractive option for NSTX-U; however, more experimental work is needed to clarify the pedestal and divertor transport and MHD physics contributing to this effect.

Both the RD and SF based divertor strategies must not only be compatible with high core performance and pedestal stability satisfying a reduced-size ELM regime, but also, importantly, have acceptable divertor heat and particle control. For active RD and SF control, details of the onset and spatial distribution of divertor heat flux footprint and radiation are important. Shown in Fig. 3 are divertor heat flux, deuterium B6 ($n = 6-2$, $\lambda$410.0 nm) brightness, and C III ($\lambda$407 nm) and C IV ($\lambda$580.9 nm) brightness profiles measured with the IR thermography,

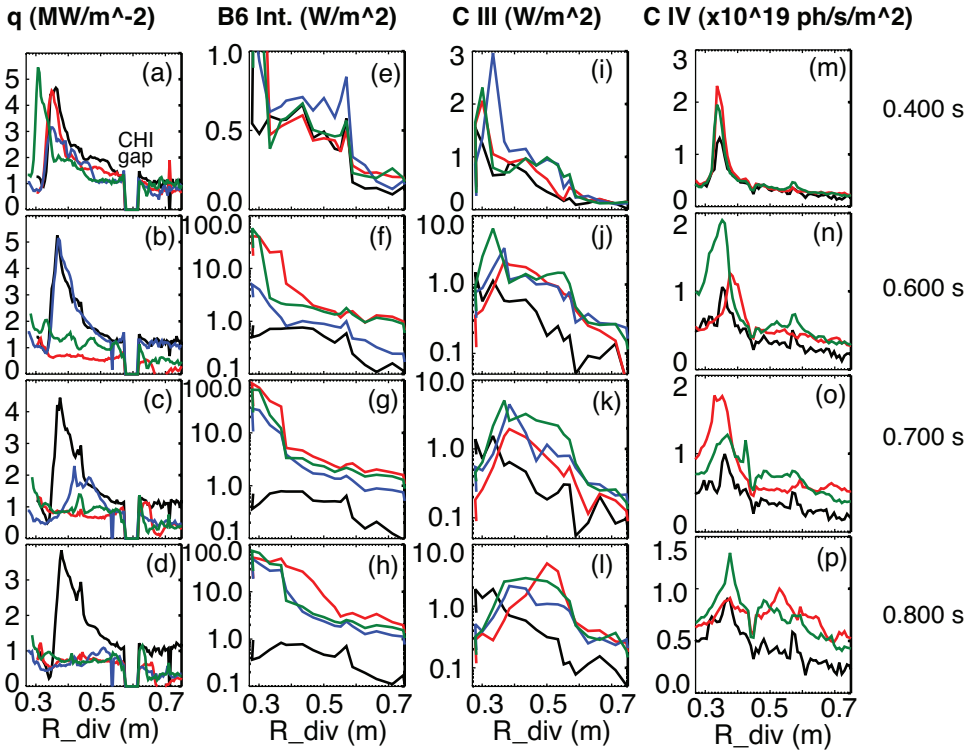


**Figure 3:** Divertor profiles measured in the four discharges at times before (0.400 s) and during and after (0.600 s, 0.700 s, 0.800 s) the onset of SF geometry and RD induced by $CD_4$ puffing. (a)-(d) - divertor heat flux; (e)-(h) - Divertor B6 intensity; ((i)-(l) - Divertor C III intensity; (m)-(p) - Divertor C IV intensity.

spectrometers and filtered cameras before (0.400 s) and during (0.600 s - 0.800 s) the radiative and SF phases. In the standard divertor phase and before the gas seeding, peak divertor heat flux was 3-5.5 MW/m$^2$. In the SF divertor, peak heat flux was reduced with or without gas seeding to about 1 MW/m$^2$: the divertor $q$ profiles were essentially flat, due to a shallow magnetic field line angle and the radiative heating from impurity radiation. The reduced $q_{div}$ region spanned about 30-50 % of the SOL power width $\lambda_{SOL}$ that was estimated to be 5-7 mm in the midplane using recent $\lambda_{SOL}$ scaling experiments [2]. In the RD discharge, peak divertor heat flux was reduced from 4-5 to 1-2 MW/m$^2$, and the reduction took place in the strike point region spanning about $\leq 20-30$ % of $\lambda_{SOL}$.

Volumetric electron-ion recombination and charge exchange are important divertor ion momentum sinks in the RD regime. The measured deuterium B6 intensity profiles were indicative of the volumetric recombination rate trend observed in the RD and SF divertor. In both cases, with and without gas seeding, the B6 intensity substantially increased, perhaps more in the SF geometry, where a longer connection length (w.r.t. mean recombination length) aided more recombination events. The B6 intensity increase suggested similarly low divertor $T_e \leq 1-2$ eV and high $n_e \geq 1\times10^{20}$ m$^{-3}$ obtained from gas seeding or geometry-induced features (e.g., [16]). It also appeared that in both the RD and SF divertor the region of enhanced recombination in the inner divertor and X-point moved toward the outer strike point region and increased throughout outer SOL during the detachment onset.

The main radiating species in a divertor with graphite PFCs at low $T_e$ are C III and C IV. in both RD and SF divertor, all spectroscopic measurements showed a significant increase in divertor carbon radiation, as shown in Figs. 2 and 3. As with recombination, C III and CIV radiation was peaked in the inner divertor and X-point regions in the standard unseeded divertor, and spread toward the outer strike point during the onset of detachment in the RD or SF divertor.

An important conclusion from the C III and C IV profiles was that the seeded SF divertor generally showed increased radiation, both in the intensity (i.e. due to the dependence of the carbon radiative cooling rate $L_C$ on $n_e, T_e$), and in the spatial extent, due to the SF divertor high-flux expansion zone.

The divertor heat flux reduction results with the RD and seeded and unseeded SF divertor are summarized in Fig. 4. The between-ELM (steady-state) peak heat flux $q_{peak}$ increased proportionally with $P_{SOL}$ in these experiments, slightly deviating from the linear scaling at higher $P_{SOL}$. Both the RD and SF divertor (with and without seeding) significantly reduced $q_{peak}$ at $P_{SOL} \sim 3$ MW. However, more experiment are needed to demonstrate these techniques at $P_{SOL} \geq 4-5$ MW for NSTX-U. In particular, additional radiating species may be considered to enhance divertor radiation in the SF divertor. It is envisioned that all graphite PFCs as well as PFC conditioning via lithium and boron coatings would be used in the initial period of NSTX-U operation [1]. The seeding gas options at this stage would be $D_2$, $CD_4$, and Ar. Nitrogen is considered incompatible with lithium coatings as it forms a stable nitrate compound; nitrogen also tends to be adsorbed to graphite surfaces. However, if NSTX-U PFCs are eventually upgraded to molybdenum and/or tungsten, $D_2$, $N_2$ and Ar could be used in the standard and SF divertor geometries.

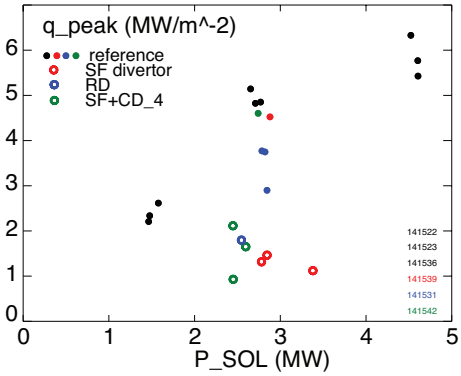


**Figure 4:** *Divertor peak heat flux $q_{peak}$ as a function of scrape-off layer power ($P_{SOL}$ for reference standard divertor discharges (filled circles) and the RD and SF divertor discharges (open circles).*

**Acknowledgments** We thank the entire NSTX Team for the technical, engineering and computer support as well as the plasma, NBI and diagnostic operations. This work was performed under the auspices of the U.S. Department of Energy under Contracts DE-AC52-07NA27344, DE AC02-09CH11466, DE-AC05-00OR22725, DE-FG02-08ER54989.

## References

[1] MENARD, J. et al., Nucl. Fusion **At press** (2012).
[2] GRAY, T. et al., J. Nucl. Mater. **415** (2011) S360.
[3] RYUTOV, D., Phys. Plasmas **14** (2007) 064502.
[4] SOUKHANOVSKII, V. et al., J. Nucl. Mater. **337-339** (2005) 475.
[5] SOUKHANOVSKII, V. et al., J. Nucl. Mater. **363-365** (2007) 432 .
[6] SOUKHANOVSKII, V. et al., Phys. Plasmas **16** (2009) 022501.
[7] SOUKHANOVSKII, V. et al., Nucl. Fusion **49** (2009) 095025.
[8] SOUKHANOVSKII, V. et al., Nucl. Fusion **51** (2011) 012001.
[9] SOUKHANOVSKII, V. A. et al., Phys. Plasmas **At press** (2012).
[10] MCLEAN, A. G. et al., Rev. Sci. Instrum. **Submitted** (2012).
[11] SOUKHANOVSKII, V. et al., Rev. Sci. Instrum. **81** (2010) 10723.
[12] SCOTTI, F. et al., Rev. Sci. Instrum. **At press** (2012).
[13] PAUL, S. F. et al., J. Nucl. Mater. **337-339** (2005) 251.
[14] MANSFIELD, D. et al., J. Nucl. Mater. **390-391** (2009) 764.
[15] MAINGI, R. et al., Phys. Rev. Lett. **103** (2009) 075001.
[16] SOUKHANOVSKII, V. et al., J. Nucl. Mater. **415** (2011) S365.